Click Here for Full Article

Numerical evaluation of alternative heat pulse probe designs and analyses

Hirotaka Saito,[1,2] Jiri Šimůnek,[1] Jan W. Hopmans,[3] and Atac Tuli[3]

[1] The heat pulse probe (HPP) has received more attention as it allows in situ, simultaneous, and automated measurements of soil hydraulic and thermal properties, as well as soil water fluxes. Although the currently used design allows many applications, changes in HPP design and analyses are needed to increase the sensitivity to smaller water fluxes. In this study, numerical simulations were used to evaluate the effects of (1) sensor locations and thermal properties of the HPP sensor body material, (2) the heater diameter and heat pulse intensity, and (3) vapor flow on HPP performance. A numerical study was carried out using the HYDRUS code for the HPP consisting of three parallel needles, spaced 6 mm apart. A heater of varying diameter in the center is surrounded by a pair of thermistor needles. Our results show that significantly different temperature responses will be obtained depending on the axial location of thermistors, and that only temperature measurements near the middle of the 33-mm-long heater fulfill the assumption of an infinite line heat source. It is shown that larger heater needle diameters allow larger heat pulses, leading to larger temperature differences between upstream and downstream thermistor needles and a higher sensitivity to water flux measurements. For example, for a standard 1-mm-diameter heater needle, ten times greater heat pulse input results in ten times greater sensitivity, but with the maximum temperature at the heater exceeding 100°C. This maximum temperature can be reduced to 80°C by increasing the heater diameter to 4 mm, while maintaining equal sensitivity. Consideration of vapor transport significantly reduced temperature increases near the heater caused by latent heat of vaporization. Larger heat pulses are beneficial for estimation of liquid water fluxes in the 1 cm d^{-1} range, provided vapor transport is considered.

Citation: Saito, H., J. Šimůnek, J. W. Hopmans, and A. Tuli (2007), Numerical evaluation of alternative heat pulse probe designs and analyses, *Water Resour. Res.*, *43*, W07408, doi:10.1029/2006WR005320.

1. Introduction

[2] Soil hydraulic and thermal properties are of great interest in many scientific and engineering applications where accurate predictions of soil water content and temperature are required as these significantly control many soil physical, chemical, and biological processes. Knowledge of both sets of properties is also required by models simulating simultaneous movement of liquid water, water vapor and heat in the vadose zone, playing a critical role in the overall water and energy balance, especially in arid or semiarid regions with generally low soil moisture content values. The heat pulse probe (HPP) has received increasing attention over the last decade as it allows in situ, direct, simultaneous, rapid, and automated measurements of both soil hydraulic and thermal parameters, as well as soil water fluxes.

[3] The dual-needle HPP allows rapid estimation of the soil thermal properties from measured temperature changes, at a fixed distance from a heater needle that approximates a line source. The original design of the dual heat pulse probe consists of two parallel 28-mm-long and 0.8-mm-diameter needles mounted to the HPP sensor body with a 6-mm separation distance [*Campbell et al.*, 1991]. In their analysis, a short known 8-s heat pulse was generated in one of the needles. An analytical solution for an infinite line source derived with an instantaneous (Dirac-type) heat pulse was used to estimate the heat capacity and volumetric water content of the surrounding soil. As the instantaneous heat pulse solution was found inadequate to estimate soil thermal diffusivity and soil thermal conductivity, *Bristow et al.* [1994] developed instead an approach on the basis of the analytical solution for a short-duration heat pulse. Their approach allowed simultaneous estimation of all three soil thermal properties; i.e., the thermal diffusivity, heat capacity, and thermal conductivity, as well as soil water content [*Bristow*, 1998].

[4] More recently, *Ren et al.* [2000] used a tri-needle HPP to indirectly estimate also the saturated water flux density from the difference in temperature changes measured downstream and upstream of the heating needle. The tri-needle HPP consists of three parallel needles positioned in a

---
[1]Department of Environmental Sciences, University of California, Riverside, California, USA.
[2]Now at Department of Ecoregion Science, Tokyo University of Agriculture and Technology, Tokyo, Japan.
[3]Department of Land, Air and Water Resources, University of California, Davis, California, USA.

common plane and mounted to the HPP sensor body with a 6-mm separation distance between the heater needle and both thermistor needles. If the three needles are aligned along the water flow direction, the difference in temperature signals between the two thermistors is used to estimate convective heat transport. Thus the basic idea is to extract information related to soil water flux from the asymmetry of the temperature responses, as measured from the downstream and upstream thermistors. *Ren et al.*'s [2000] analytical solution depended on the maximum temperature difference between the two thermistor needles to estimate water flux density. While measured and predicted temperature signals agreed well for the sandy soil, significant deviations occurred for the sandy loam and clay loam that could not be explained, especially if water flux densities were small. *Wang et al.* [2002] later developed a simple mathematical analysis using the ratio of temperature changes recorded at the upstream and downstream sensors. Although their approach eliminated the complicated numerical integration [*Ren et al.*, 2000], the ratio method systematically underestimated saturated soil water fluxes [*Ochsner et al.*, 2005]. *Gao et al.* [2006] recently hypothesized that this underestimation at high water fluxes may be caused by bypass water flow along the column walls (i.e., the wall flow effect). *Gao et al.* [2006] developed a correction factor that considerably improved predictions of saturated water flow.

[5] Several recent studies demonstrated the applicability of the HPP method to analyze unsaturated water flow [*Hopmans et al.*, 2002; *Mori et al.*, 2003, 2005; *Mortensen et al.*, 2006]. While *Hopmans et al.* [2002] considered the tri-needle HPP, *Mori et al.* [2003, 2005] and *Mortensen et al.* [2006] used a multifunctional heat pulse probe (MFHPP), which was developed to evaluate simultaneously coupled water, heat, and solute transport in unsaturated soils. Unlike most other studies that relied on analytical solutions of heat transport, *Hopmans et al.* [2002] used a numerical model to simultaneously evaluate the soil hydraulic and thermal properties, as well as water fluxes. *Mortensen et al.* [2006] later extended this numerical approach to estimate thermal, hydraulic, and solute transport properties using the MFHPP. *Hopmans et al.* [2002] also investigated the possible effects of dispersive heat transport due to local pore water variations to explain discrepancies between measured and predicted temperature responses for increasing water flux densities. They suggested including an additional thermistor in the transverse direction to water flow to account for the dispersive heat flux. Although the MFHPP developed by *Mori et al.* [2003] was designed to have four thermistor needles around the heating probe, they used the same analysis as used with the tri-needle HPP.

[6] According to *Mori et al.* [2005], horizontal thermistors can be used to estimate the thermal diffusivity, if the water flux is small enough so that the convective heat transport can be neglected. In the work of *Mori et al.* [2005], unsaturated water fluxes were estimated using the multistep outflow experiment combined with the analytical solution of *Ren et al.* [2000] that considers convective heat transport. Despite obtaining accurate predictions of saturated water fluxes, unsaturated water fluxes were generally overestimated. Differences between measured and predicted values increased specially for water fluxes below 0.1 m d^{-1}. Unlike *Mori et al.* [2003, 2005] who relied only on analy-

tical solutions to estimate soil thermal and hydraulic parameters, *Mortensen et al.* [2006] used a numerical inverse analysis to analyze MFHPP measurements. *Mortensen et al.* [2006] used the flexibility of the numerical inverse analysis to combine different types of information to simultaneously estimate thermal, hydraulic, and solute transport properties. In general, the estimated transport properties and saturated/unsaturated water flux densities were in good agreement with independently measured values. Their study showed that the MFHPP combined with the (inverse) numerical approach is a promising methodology to simultaneously estimate soil hydraulic, thermal, and solute transport properties. An important advantage of the numerical approach in analyzing data collected with the HPP is the elimination of constraints on needle geometry as imposed by analytical solutions. With user-friendly and powerful numerical codes simulating coupled water, heat, and solute transport, it is expected that an increasing number of studies will adopt numerical approaches in analyzing HPP (or MFHPP) and other measurements.

[7] Although significant advances occurred during the last decade in applications of the HPP [*Ren et al.*, 2000; *Mori et al.*, 2003, 2005; *Ochsner et al.*, 2005; *Mortensen et al.*, 2006] and in understanding of the underlying theory [*Kluitenberg et al.*, 1995; *Knight and Kluitenberg*, 2005], it is rather surprising that the HPP design and operation (i.e., about 30-mm-long and 1-mm-diameter probes aligned parallel with 6-mm spacing distance, using a heat pulse of about 60 W m^{-1} for 8 s) have not changed much from those originally presented by *Campbell et al.* [1991]. With the current design and operation, the lower limit of accurate estimations of the water flux density is 0.06 m d^{-1}, for a temperature measurement resolution of about 0.01°C [*Ren et al.*, 2000; *Mortensen et al.*, 2006]. To increase the sensitivity of HPP to smaller water fluxes, changes in HPP design, operation, and analysis are needed. Additionally, the error analysis by *Kluitenberg et al.* [1995] showed the sensitivity of soil thermal properties on needle spacings: 2% error in the spacing between heater and thermistors led to 4% error in the estimated thermal diffusivity and heat capacity. Therefore it is very important to use rigid probes to minimize changes in spacing distances during their installation. For that purpose, shorter thermistor needles were proposed by *Mori et al.* [2003] to minimize deflection of needles during installation. However, it is expected that thermistor readings close to the HPP body may be affected by its thermal properties. While thinner needles will distort the flow field to a lesser extent, they can create sharp temperature increases for larger heat pulses, leading to evaporation and boiling of soil water around the heater needle. In contrast, thicker needles will increasingly distort the flow field, but will reduce temperature increases around the heater for equal heat pulse intensities. Proposed geometrical changes and changes in HPP operation can affect the HPP performance, and therefore need to be fully evaluated.

[8] Increased temperatures around the heater needle during the release of the heat pulse will create significant temperature gradients, inducing both liquid water and water vapor transport in the direction of decreasing temperatures. High temperatures may lead to water evaporating around the heater and reducing temperatures generated by the released heat, thereby affecting heat transport. Yet, the

Figure 1. Schematic showing the heat pulse probe (HPP) with a total of 16 thermistors. Distances between the centers of the heater and thermistor needles are 6 mm.

simultaneous movement of liquid water, water vapor, and heat has not been considered in the HPP analysis.

[9] The main objectives of this study therefore are to numerically evaluate (1) effects of thermistor locations of the heat pulse probe and thermal properties of the HPP sensor body material, (2) effects of the heater diameter and heat pulse intensity on measured temperature responses, and (3) effects of vapor flow on HPP performance. While the first objective is achieved by numerically solving the heat transport equation by considering thermal conduction only, the second objective also considers convection of sensible heat. Finally, the third objective is achieved by numerically solving coupled movement of liquid water, water vapor and heat. The first objective is achieved using both measured and numerically generated data.

2. Experimental HPP

[10] Prior to numerical evaluation of the effects of thermistors location and HPP design on measurement sensitivity, we verified the presented numerical approach experimentally after construction of a multithermistor HPP. Figure 1 shows a schematic diagram of the specific five-needle HPP constructed to evaluate influence of thermistor position and sensor body material. With the exception of the larger number of thermistors and the elimination of the Wenner array electrodes, the fabrication of the multithermistor HPP is similar to the MFHPP presented by *Mori et al.* [2005] and *Mortensen et al.* [2006]. In addition to a 26-mm-long central heater needle (LN-2), this specific HPP includes two short 13-mm (SN-5 and SN-6) and two long 26-mm thermistor needles (LN-1 and LN-3). Each thermistor needle incorporates three SN or four LN thermistors. Additional thermistors were installed on the outside of the heater needle (5) and in the acetal Delrin base of the sensor body (16), 6 mm away from SN-6 (Figure 1). All needles were constructed from 1.27-mm O.D. and 0.84-mm I.D. stainless steel hollow tube [*Mori et al.*, 2003]. The multithermistor HPP included a total of 16 0.46-mm-diameter thermistors (10 kΩ resistance at 25°C with 0.004°C precision; Model 10K3MCD1, Betatherm Corporation, Shrewsbury, Massachusetts). After insertion of the thermistors in the needles, the available hollow space was filled with Omegabond 101 epoxy (Omega Engineering, Stamford, Connecticut), which has a relatively high thermal conductivity and is a good electrical insulator [*Mori et al.*, 2003].

Table 1. Measured Thermal Properties of Delrin That Was Used for the Body Material of the HPP in Figure 1 (Section 3.1)[a]

	Delrin			
	23°C	40°C	60°C	80°C
Thermal conductivity, W m^{-1} K^{-1}	0.364	0.372	0.378	0.380
Heat capacity, MJ m^{-3} K^{-1}	1.8	2.0	2.1	2.3
Thermal diffusivity[b], $\times 10^{-6}$ m^2 s^{-1}	0.20	0.19	0.18	0.16

[a]HPP is heat pulse probe. Density of Delrin is 1.41 gm cm^{-3}.
[b]Thermal diffusivity is defined as the ratio of thermal conductivity to heat capacity.

All five needles were secured through predrilled holes in a 50.8-mm-diameter and 7.9-mm-thick Delrin plug. All 34 lead wires were soldered to 34 corresponding wires of two 24 AWG shielded multiconductor cables (Belden, electronics Division, Richmond, Indiana). The multiconductor cables were held in place by another 20-mm-long Delrin plug that closed the air-filled space within the sensor body. The thermal properties of the Delrin, measured by TPRL Incorporated (3080 Kent Avenue, West Lafayette, Indiana 47906) for a range of temperatures using differential scanning calorimetry (specific heat) and laser flash diffusivity method (thermal diffusivity), are listed in Table 1. Reasons for using Delrin were its high tensile strength and the relative ease by which it can be machined. Since all parts were screwed together, it can be easily disassembled, so that electrical circuitry can be checked and needles can be interchanged in case of malfunctioning.

[11] The heater was constructed by inserting two loops of 79-μm-diameter 209.7 Ω m^{-1} Nichrome 80 alloy enameled resistance wire (Pelican Wire Company, Incorporated, Naples, Florida) into the heater needle (LN-2). Heat input and temperature logging of all thermistors was controlled by a CR10 datalogger (Campbell Scientific Incorporated), as presented by *Mori et al.* [2003].

[12] To test its functionality and for calibration purposes, the multithermistor HPP was evaluated in a 4 g L^{-1} agar solution. As was done by *Mori et al.* [2003], the agar test was used to determine the effective separation distance (r_{eff}) of all thermistor needles and the heater, assuming that the thermal properties of the agar solution are equal to those of water. This was done by fitting measured heat pulse responses for thermistors 2, 6, 10, and 13 to the solution of heat conduction equation for an infinite line heat source [*Mori et al.*, 2003, 2005]. As in the work of *Mori et al.* [2003], we also determined the r_{eff} in full saturation of Tottori sand with water. Values for r_{eff} were between 5.90 and 6.30 mm, and were equal to values determined by *Mori et al.* [2003].

[13] Temperature responses of a few selected thermistors were used to validate the sensitivity results with the inverse modeling module of the HYDRUS model [*Šimůnek et al.*, 2006], as was done by *Mortensen et al.* [2006]. In this module, the Levenberg-Marquardt algorithm is used for parameter optimization. Since no water flow occurred in this experiment, only heat conduction was considered. The objective function minimized in the optimization was defined as the sum of weighted squared residuals between measured and simulated temperatures [*Mortensen et al.*, 2006]. For this purpose, temperature changes at all thermis-

tors were measured in agar solutions after a 103.59 W m^{-1} heat pulse for 8 s.

3. Numerical Analysis

[14] Since an axisymmetrical three-dimensional solution can be achieved with a two-dimensional model, only a two-dimensional formulation will be presented. Perfect thermal contact was assumed in all numerical calculations at interfaces between HPP needles and the surrounding soil. Although it has been known that an imperfect thermal contact can have a profound impact on heat transport through the interface, theoretical solutions for HPP have always been derived with the assumption of perfect thermal contact [e.g., *Ren et al.*, 2000]. All numerical calculations were carried out using the HYDRUS software program [*Šimůnek et al.*, 2006].

3.1. Sensor Locations and Thermal Properties of HPP

[15] The first part investigates the effects of thermistor locations and HPP body material on temperature measurements. This simulation was conducted independently from the experimental study discussed earlier in the paper. The axisymmetric simulation domain had a radius of 20 mm from the center of the heater and a height of 68 mm (Figure 2). To preserve the axisymmetricity of the problem, only thermal conduction was considered. The governing equation of heat transport in the axisymmetric domain to be solved is described by

$$C_p \frac{\partial T}{\partial t} = \frac{1}{r} \frac{\partial}{\partial r}\left(r \lambda_0(\theta) \frac{\partial T}{\partial r}\right) + \frac{\partial}{\partial z}\left(\lambda_0(\theta) \frac{\partial T}{\partial z}\right) \qquad (1)$$

where r is the radial distance from the center of the domain (m), z is the vertical coordinate (m), C_p is the volumetric heat capacity of the moist soil (J m^{-3} K^{-1}), defined as the sum of volumetric heat capacities of the soil and water multiplied by their volumetric fractions, T is temperature (K), and $\lambda_0(\theta)$ is the soil's isotropic thermal conductivity (diagonal tensor) (W m^{-1} K^{-1}), accounting for the tortuosity and water content of the porous medium, as described by a simple equation given by *Chung and Horton* [1987]:

$$\lambda_0(\theta) = b_1 + b_2\theta + b_3\theta^{0.5} \qquad (2)$$

where θ defines the soil volumetric water content (m^3 m^{-3}), and b_1, b_2, and b_3 are empirical regression parameters (W m^{-1} K^{-1}).

[16] Figure 2 shows the finite element mesh for the computational domain with gradually increasing size of the finite elements away from the heater. The simulation domain consisted of two materials: the soil and the HPP body. The soil was considered uniform and homogeneous, having an initial temperature of 20°C, a saturated water content of 0.43 m^3 m^{-3}, with a solid phase fraction of 0.57 m^3 m^{-3} and a thermal conductivity for a loam ($b_1 = 0.243$ W m^{-1} K^{-1}, $b_2 = 0.393$ W m^{-1} K^{-1}, and $b_3 = 1.534$ W m^{-1} K^{-1} in equation (2), [*Chung and Horton*, 1987]). Volumetric heat capacities of the solid phase, C_s, and liquid water, C_w, were 1.92 and 4.18 MJ m^{-3} K^{-1}, respectively. The thermal properties of the soil are summarized in Table 2. The body of the HPP (lower 18 mm in
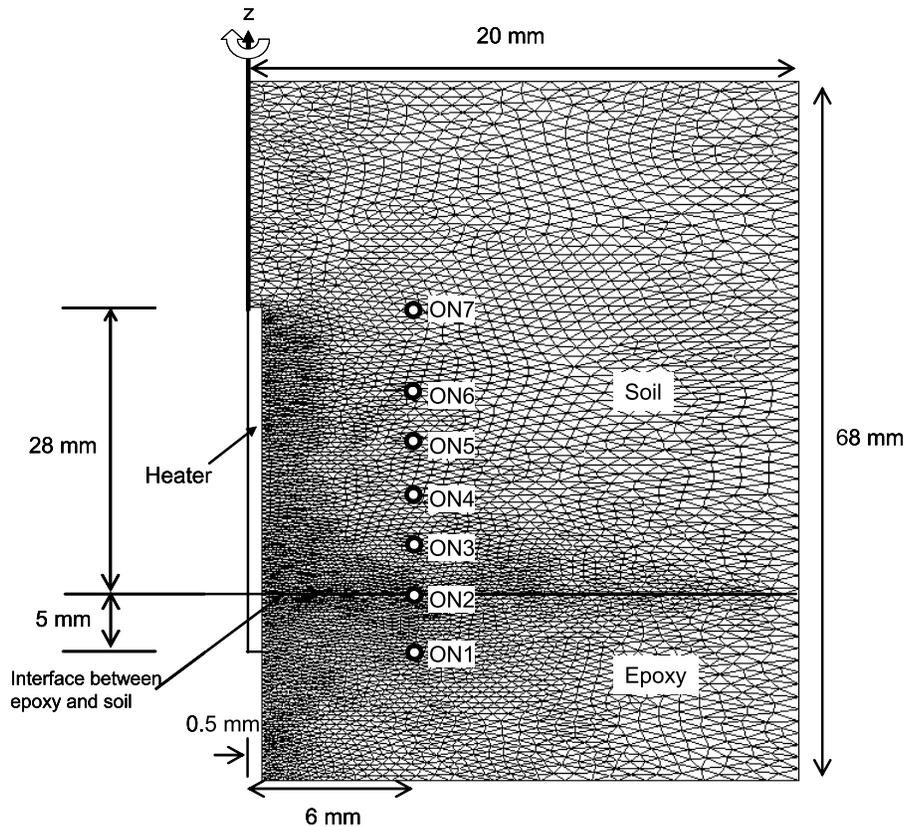
Figure 2. A finite element mesh used to investigate the effects of sensor locations and heat pulse probe sensor materials. Seven observation nodes (ON) are placed along the assumed thermistor probe, located 6 mm away and parallel to the heater probe. The transport domain is axisymmetrical around the vertical axis.

Figure 2) was assumed to be made from either thermally conductive or nonconductive epoxy following *Ham and Benson* [2004]. Thermal properties of both epoxies are listed in Table 3. The heat pulse was applied at the boundary nodes, corresponding with the wall of the heater needle.

[17] Following the standard geometry of the HPP, the total length of the heater was 33 mm, of which 5 mm was imbedded in the epoxy material of the sensor body, and the diameter was 1 mm. To mimic standard experiments, a 60 W m^{-1} heat pulse was applied to the heater for 8 s at the start of each model simulation. The heat transport module of HYDRUS was modified by adding a zero-order source term to represent the heat pulse boundary condition in finite element nodes at the surface of the heater (similarly as by *Hopmans et al.* [2002]). A given heat pulse was then uniformly distributed along these nodes (Figure 2). The zero temperature gradient boundary condition was used in the remaining boundary nodes. Temperature changes were numerically recorded for about 300 s at seven observation nodes, located along the assumed thermistor needle, 6 mm away from the heater. One observation node (ON1) was positioned 5 mm in the sensor body, one observation node (ON2) was located at the soil-epoxy interface, and additional five observation nodes were placed in the soil (ON3 through ON7 at 5, 10, 15, 20, and 28 mm away from the soil-epoxy interface, respectively: Figure 2). As the heater needle was inserted 5 mm into the body of the HPP sensor, we could evaluate the effects of heating the bottom section of the heater on temperature changes along the sensor. Thus

a total of four simulations were conducted that considered thermally conductive epoxy with (case (a)) and without (case (c)) heating of the sensor body, and thermally nonconductive epoxy with (case (b)) and without (case (d)) heating of the sensor body. The numerical solutions for these four cases were compared with the infinite line heat source analytical solution that uses the two-dimensional radially symmetric transport domain perpendicular to the heater probe, as used by *Hopmans et al.* [2002].

[18] Another factor that may affect the HPP performance is the axial conduction of heat in the thermistor needle as they are usually built from a thermally much more conductive material (stainless steel) than the surrounding soil. If the thermal conductivity of the sensor needle was infinite, the heat would be redistributed instantaneously along the needle and thermistors located at any position would measure the

Table 2. Thermal Properties of the Soil Used in This Study (Sections 3.1, 3.2, and 3.3)

Parameter	Units	Value	References
b_1	W m^{-1} K^{-1}	0.243	*Chung and Horton* [1987]
b_2	W m^{-1} K^{-1}	0.393	
b_3	W m^{-1} K^{-1}	1.534	
C_w	MJ m^{-3} K^{-1}	1.92	
C_s	MJ m^{-3} K^{-1}	4.18	
β_L	M	0.00221	*Hopmans et al.* [2002]
β_T	M	0.1 β_L	

Table 3. Thermal Properties of Epoxies Used for the Heat Pulse Probe Body (Section 3.1), Adapted From *Ham and Benson* [2004]

Epoxy	Thermal Conductivity, W m^{-1} K^{-1}	Heat Capacity, MJ m^{-3} K^{-1}
Thermally conductive	0.6	2.9
Thermally nonconductive	0.2	1.7

same temperature. However, the axial conduction of heat in the sensor adds a third dimension to the problem and cannot thus be evaluated simultaneously with the heat transport from the heater using axisymmetrical calculations. Had a narrow strip with larger heat conductivity been specified at a location of observation nodes in the domain shown in Figure 2, this would have represented, because of the axisymmetricity of the problem, a conductive cylinder, rather than a needle. To avoid the need for a full three-dimensional simulation, an axisymmetric simulation domain that consisted only of the thermistor needle and the surrounding soil was used to investigate the influence of the axial conduction of heat on temperature profiles within the thermistor needle. Figure 3 shows the finite element mesh for the resulting computational domain. The small layer of the soil (0.25 mm thickness) had to be included into the transport domain so that heat could be redistributed within a needle and back to the soil. If the boundary temperature was imposed directly at the surface of the sensor needle, such redistribution would not have been possible. The thermistor needle was assumed to have typical dimensions of 1-mm diameter and 33-mm length. The thermal properties of the soil were the same as above, while the thermal properties of typical stainless steel, whose thermal conductivity is one order of magnitude greater (16.3 W m^{-1} K^{-1}) than that of the soil, were used for the thermistor needle, as HPP needles are usually made from it. Since this numerical experiment was conducted solely to demonstrate the impact of the axial conduction, any material with much greater thermal conductivity than that of the soil could be used. Calculated temperatures at seven observation nodes in Figure 2 for case (a) and the interpolated values were prescribed as boundary conditions along the outside boundary of the transport domain. Temperature changes at three locations correspond to ON2, ON4, and ON6 in Figure 2 (5, 15, and 25 mm from the bottom of the domain as shown in Figure 3), in the center of the thermistor needle were calculated and compared to those at the domain boundary.

3.2. Heater Size and Heat Pulse Intensity

[19] The effects of the diameter of the heater needle and heat pulse intensity on HPP performance was studied using a two-dimensional transport domain perpendicular to the heat pulse probes (Figure 4). Because we consider heat convection by steady state liquid water flow in this case, the governing equation of heat transport is described by

$$C_p \frac{\partial T}{\partial t} = \nabla[\lambda(\theta)\nabla T] - C_w q_l \nabla T \qquad (3)$$

where q_l is the flux density (m s^{-1}) of liquid water, C_w is the volumetric heat capacity of the liquid water (J m^{-3} K^{-1}), and $\lambda(\theta)$ now denotes the soil's apparent thermal conductivity (J m^{-1} s^{-1} K^{-1}) that combines the soil thermal

conductivity in the absence of flow, $\lambda_0(\theta)$, with a macro-dispersivity term, which is assumed to be a linear function of velocity [*de Marsily*, 1986; *Hopmans et al.*, 2002]. The apparent thermal conductivity for the two-dimensional heat transport equation is expressed as [*Šimůnek and Suarez*, 1993]:

$$\lambda_{ij}(\theta) = \lambda_0(\theta)\delta_{ij} + \delta_{ij}\beta_T C_w|q_l| + (\beta_L - \beta_T)C_w\frac{q_{l,j}q_{l,i}}{|q_l|} \qquad (4)$$

where δ_{ij} is the Kronecker delta ($\delta_{ij} = 1$ if $i = j$, and $\delta_{ij} \neq 0$ otherwise), β_L and β_T are the longitudinal and transverse thermal dispersivities (m), respectively (Table 2). The liquid water flux q_l (m s^{-1}) is calculated using a two-dimensional isothermal Darcian equation:

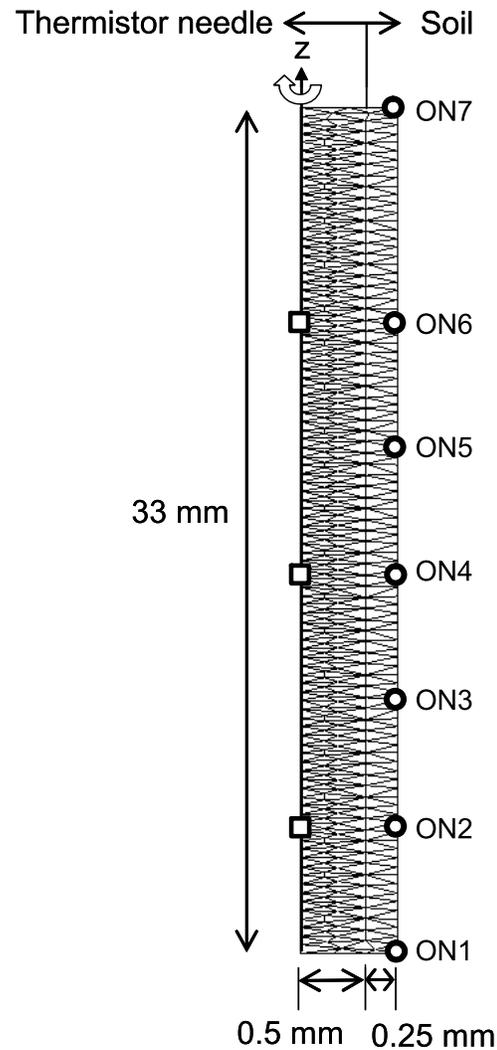$$q_l = K_{lh}\nabla h + K_{lh}\vec{k} \qquad (5)$$

Figure 3. A finite element mesh used to investigate the effects of axial conduction of heat in the thermistor needle. The transport domain is axisymmetrical around the vertical axis. Open squares indicate locations where temperature changes were observed, while open circles correspond to observation nodes (ON) in Figure 2.
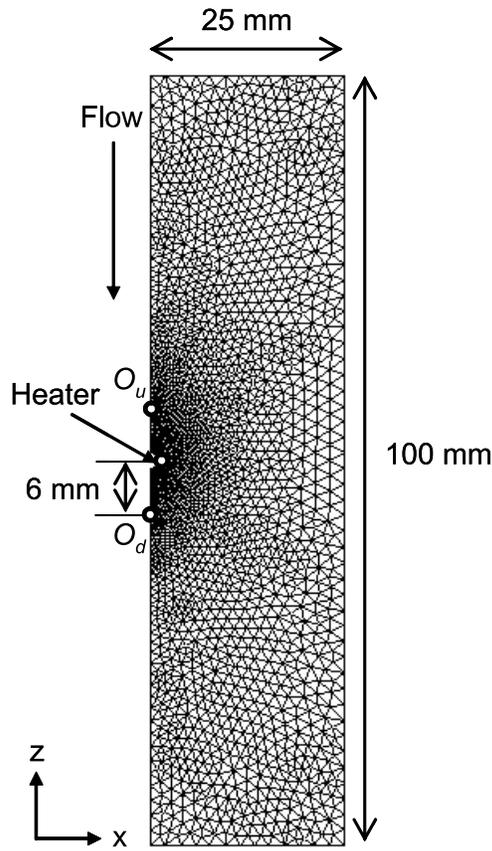
Figure 4. A finite element mesh used to investigate the effects of the heater size and heat pulse intensity. Effects of the vapor transport on the HPP performance was studied using this two-dimensional transport domain. Temperatures were recorded at three observation nodes (open circles), O_u, and O_d representing upstream and downstream probes, respectively, as well as near the heater.

where h is the pressure head (m), $\vec{k}$ is the vertical unit vector, and K_{lh} is the (isothermal) hydraulic conductivity (m s^{-1}). For isotropic conditions, K_{lh} is a tensor with zero nondiagonal terms. The governing equation for the liquid water flow is then given by the Richards equation as

$$\frac{\partial \theta}{\partial t} = \nabla \left[K_{lh} \nabla h + K_{lh} \vec{k} \right] \qquad (6)$$

[20] The pore size distribution model of *Mualem* [1976] was used to predict the isothermal unsaturated hydraulic conductivity function, K_{lh}, from the saturated hydraulic conductivity and the *van Genuchten*'s [1980] model parameters of the soil water retention curve (7) and (8):

$$K_{lh}(h) = K_s S_e^{0.5} \left[1 - \left(1 - S_e^{1/m} \right)^m \right]^2 \qquad (7)$$

$$S_e(h) = \frac{\theta - \theta_r}{\theta_s - \theta_r} = \begin{cases} \dfrac{1}{[1 + |\alpha h|^n]^m} & h < 0 \\ 1 & h \geq 0 \end{cases} \qquad (8)$$

where K_s is the saturated hydraulic conductivity (m s^{-1}), S_e is the effective saturation (−), θ_s and θ_r are the saturated and residual water contents (m^3 m^{-3}), respectively; and α (m^{-1}), n (−), and m (= 1 − 1/n) are empirical shape parameters.

[21] In this numerical experiment the distance between the center of the heater and both thermistor needles (upstream and downstream) was held constant at 6 mm, so that the size of the radiated heat pulse at the sensor needle is consistent between different heater sizes. The duration of the heat pulse was 8 s, assuming an infinite and uniform heater source. The initial temperature was 20°C for the entire domain. The bulk water flux, except around the heater, was assumed uniform and unidirectional, parallel with the vertical axis, by specifying identical flux boundary conditions at the top and bottom of the transport domain and assuming a zero horizontal flux at the vertical sides of the domain. While water flowing into the domain at the top was assumed to have a 20°C temperature, the remaining domain boundaries were simulated with a second-type boundary condition of zero temperature gradient. A specified heat pulse was distributed uniformly across all nodes of the heater.

[22] Temperatures were observed at three observation nodes: O_u, O_d, and at the heater itself (Figure 4). The impact of heater diameter (d) and heat pulse intensity (H) for a range of water fluxes (q) and water contents (θ) (Table 4) was investigated. Since the effect of the vapor phase was not considered, target water fluxes and water contents were artificially established by assuming saturated water flow. For example, to obtain a water flux of 0.1 m d^{-1} and the volumetric water content of 0.3 m^3 m^{-3}, the soil was assumed to be saturated, having the saturated hydraulic conductivity K_s equal to 0.1 m d^{-1}, the corresponding saturated water content of 0.3 m^3 m^{-3}, and with all other remaining parameters unchanged.

3.3. Vapor Transport

[23] To evaluate the effects of the coupled movement of liquid water, water vapor, and heat, selected simulations from section 3.2 were reevaluated, while considering phase changes. The governing equation accounting for heat conduction, convection of sensible heat by movement of liquid water and water vapor, and transfer of latent heat by diffusion of water vapor is given by [*Nassar and Horton*, 1992]

$$C_p \frac{\partial T}{\partial t} + L_0 \frac{\partial \theta_v}{\partial t} = \nabla[\lambda(\theta)\nabla T] - (L_0 + C_v T)\nabla q_v - C_v q_v \nabla T \\ - C_w T \nabla q_l - C_w q_l \nabla T \qquad (9)$$

where L_0 is the volumetric latent heat of vaporization of liquid water (J m^{-3}), θ_v is the volumetric water vapor

Table 4. Values of Variables Used in Numerical Simulations Investigating the Effects of the Heater Diameter and Heat Pulse Intensity[a]

Variables	Values
Diameter, d, mm	1, 2, 4
Flux, q, m d^{-1}	0.01, 0.1, 0.5, 1, 10
Water content, θ, m^3 m^{-3}	0.3, 0.4, 0.5, 0.6
HPP intensity, H, W m^{-1}	60, 150, 300, 600

[a]All possible 240 combinations were considered (section 3.2).

Table 5. Soil Isothermal and Thermal Conductivity Models and Their Parameter Values[a]

Models		Parameters	Description	Values
K_{lT}	$K_{lh}\left(hG_{wT}\frac{1}{\gamma_0}\frac{d\gamma}{dT}\right)$	G_{wT} (−)	gain factor	7.0
		γ_0, g s^{-2}	surface tension of soil water at 25°C	71.89
		γ, g s^{-2}	surface tension of soil water (= $75.6 - 0.1425T - 2.38 \cdot 10^{-4}T^2$)	...
K_{vh}	$\frac{D}{\rho_w}\rho_{sv}\frac{Mg}{RT}H_r$	D, m^2 s^{-1}	vapor diffusivity in soil (= $\tau\theta_a D_a$)	...
		ρ_{sv}, kg m^{-3}	saturated vapor density	...
		M, kg mol^{-1}	molecular weight of water	0.018015
		g, m s^{-2}	gravitational acceleration	9.81
		R, J mol^{-1}K^{-1}	universal gas constant	8.314
		H_r (−)	relative humidity	...
		τ (−)	tortuosity factor $\left(= \dfrac{\theta_a^{7/3}}{\theta_s^2}\right)$	...
		D_a, m^2 s^{-1}	diffusivity of vapor in air $\left(= 2.12 \cdot 10^{-5}\left(\dfrac{T}{273.15}\right)^2\right)$	...
		θ_a, m^3 m^{-3}	air filled porosity	...
K_{vT}	$\frac{D}{\rho_w}\eta H_r\frac{d\rho_{sv}}{dT}$	η (−)	enhancement factor $\left(= 9.5 + 3\dfrac{\theta}{\theta_s} - 8.5\exp\left\{-\left[\left(1+\dfrac{2.6}{\sqrt{f_c}}\right)\dfrac{\theta}{\theta_s}\right]^4\right\}\right)$	...
		f_c (−)	mass fraction of clay	0.02

[a]From *Saito et al.* [2006]; section 3.3.

content (expressed as an equivalent water content, (m^3 m^{-3})), C_v is the volumetric heat capacity of the water vapor (J m^{-3} K^{-1}), and q_v is the water vapor flux density (m s^{-1}). When coupled heat transport is considered, both liquid water (q_l) and water vapor (q_v) fluxes are defined as the sum of isothermal and thermal fluxes, due to pressure head and temperature gradients, respectively [*Philip and de Vries*, 1957; *Nassar and Horton*, 1992]:

$$q_l = q_{lh} + q_{lT} = -K_{lh}\nabla h - K_{lh}\vec{k} - K_{lT}\nabla T \qquad (10)$$

$$q_v = q_{vh} + q_{vT} = -K_{vh}\nabla h - K_{vT}\nabla T \qquad (11)$$

where q_{lh} and q_{lT} are isothermal and thermal liquid water flux densities (m s^{-1}), respectively; q_{vh} and q_{vT} are isothermal and thermal water vapor flux densities (m s^{-1}), respectively; h is the pressure head (m), $\vec{k}$ is the vertical unit vector, T is the temperature (K), and K_{lh} (m s^{-1}) and K_{lT} (m^2 K^{-1} s^{-1}) are the (isothermal and thermal) hydraulic conductivities for liquid phase fluxes due to gradients in h and T, respectively; and K_{vh} (m s^{-1}) and K_{vT} (m^2 K^{-1} s^{-1}) are the isothermal and thermal vapor hydraulic conductivities (diagonal tensors), respectively. The governing liquid water and water vapor flow equation is then given by

$$\frac{\partial\theta}{\partial t} = \nabla\left[K_{lh}\nabla h + K_{lh}\vec{k} + K_{lT}\nabla T + K_{vh}\nabla h + K_{vT}\nabla T\right]$$
$$= \nabla\left[K_{Th}\nabla h + K_{lh}\vec{k} + K_{TT}\nabla T\right] \qquad (12)$$

where K_{Th} (m s^{-1}) and K_{TT} (m^2 K^{-1} s^{-1}) are the isothermal and thermal total hydraulic conductivities, respectively, and where

$$K_{Th} = K_{lh} + K_{vh} \qquad (13)$$

$$K_{TT} = K_{lT} + K_{vT} \qquad (14)$$

To calculate values of K_{lT}, K_{vh} and K_{vT}, standard models, summarized together with associated parameters in Table 5, were used [*Saito et al.*, 2006].

[24] The simulation domain was identical to that of section 3.2 (Figure 4). However, as now the soil domain includes the air phase (the soil is unsaturated) to allow for vapor transport, the soil hydraulic properties were different. Instead, simulations were carried out for a sandy soil (K_s = 71.3 or 713.0 m d^{-1}, θ_s = 0.43 m^3 m^{-3}, θ_r = 0.045 m^3 m^{-3}, α = 14.5 m^{-1}, and n = 2.6). The water content corresponding to the unsaturated hydraulic conductivity equal to the target water flux was then calculated from the van Genuchten-Mualem model (7). This water content was used as the initial water content with the target flux used as a flux boundary condition for both top and bottom boundaries. Remaining boundary conditions for water flow and heat transport were exactly the same as those used in section 3.2. Because of the induced vapor transport, water content values and both liquid water and vapor fluxes are affected by the heat pulse magnitude around the heater. Numerical experiments included simulations with and without vapor transport for different heater diameters, water fluxes, water contents, and heat pulse intensities (Table 6). Water contents listed in Table 6 were uniquely determined from the target water fluxes. For example, if the target water flux is 0.1 m d^{-1}, the corresponding water content calculated from the van Genuchten-Mualem model (7) is 0.197 (effective saturation of 0.395).

4. Results and Discussion

4.1. Sensor Location and HPP Body Material

4.1.1. Experiment

[25] Figure 5 shows observed temperature changes at thermistors 13, 14, and 15 (Figure 1) and those simultaneously fitted to observed values to estimate thermal con-

Table 6. Values of Variables Used in Numerical Simulations Investigating the Effects of Vapor Transport (Section 3.3)[a]

Variables	Values
Diameter, d, mm	1, 2, 4
Flux, q, m d^{-1}	0.01, 0.1, 1, 10[b]
Water content[c], θ, m^3 m^{-3}	0.128, 0.197, 0.315[d]
HPP intensity, H, W m^{-1}	60, 150, 300, 600

[a]All possible 48 simulations were conducted.
[b]Flux of 0.5 m d^{-1} used in Table 4 is not considered here.
[c]Water contents were calculated for given soil hydraulic properties from specified flux.
[d]The water content of 0.315 was used twice for the saturated hydraulic conductivity of 71.3 and 713 m d^{-1}.
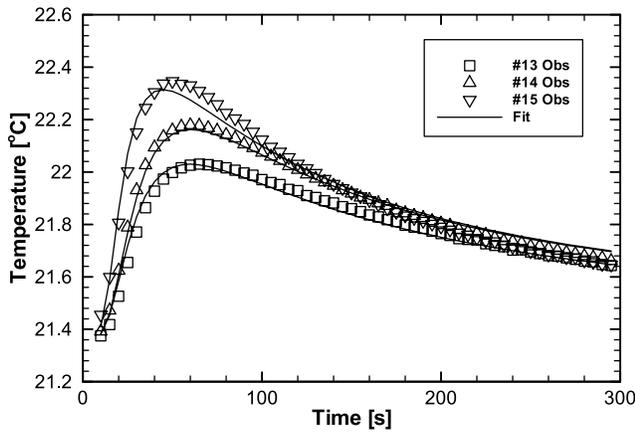
Figure 5. Temperature changes in agar solution observed at three thermistors (13, 14, and 15) along one of the short needles, SN-6, of the HPP of Figure 1, and those inversely fitted using HYDRUS.

ductivity and heat capacity of the HPP body (Delrin). The simulation domain was similar to Figure 2 with slightly different dimensions and different materials. For example, thermistor 13 of the experimental SN-6 is 13.0 mm from the sensor base (Figure 1), whereas thermistor at ON5 of the simulation domain used in the sensitivity analysis (Figure 2) is 15.0 mm from the Delrin base material of the sensor body. Although the heater wire is looped twice through most of the heater needle, there is only a single loop

embedded in the Delrin sensor body. To account for this difference in heater wire length, the heat pulse in the numerical study was applied to only 4 mm of the HPP body. While fitted temperatures matched observed temperatures well, especially those in the agar solution (thermistors 13 and 14), temperature changes in the Delrin sensor body (thermistor 15) did not correspond well. Estimated thermal conductivity and heat capacity of the Delrin were 0.201 W m^{-1} K^{-1} and 1.2 MJ m^{-3} K^{-1}, respectively. These values are about half of the independently measured values (Table 1), though the estimated thermal diffusivity of 0.17 × 10^{-6} m^2 s^{-1} is relatively close to the measured value. We are uncertain at this time what caused this large difference between measured and fitted thermal properties of the Delrin, as we did not explicitly calibrate for thermistor 15 in the sensor body, as we did for the needle thermistors. Most likely, estimated thermal properties of the Delrin were biased, because the heat pulse was applied to only 4 mm of the HPP body. However, our results suggest that thermal properties of the HPP body need to be carefully determined, if thermistors close or in the HPP sensor body are used for soil thermal measurements. In practice though, estimating thermal properties of the HPP body is usually not a goal, but is rather done during calibration. The impact of the discrepancy between observed and fitted thermal properties of the HPP body observed in this study therefore should not be significant for soil thermal property measurements.

4.1.2. Numerical Simulations

[26] Figure 6 shows temperature changes at the seven observation nodes (ON's) along the sensor needle for

Figure 6. Temperature changes at seven observation nodes (ON1–ON7) along the sensor probe for different HPP sensor body materials, with and without heating of the sensor body. The numerical solution for the infinite line source is plotted by the open circles.
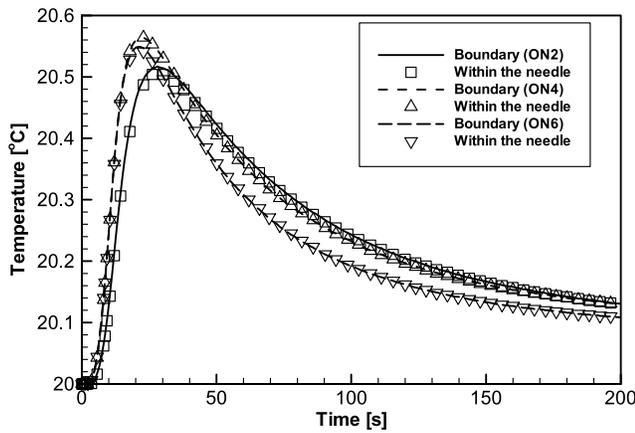
Figure 7. Temperatures (open symbols) at three locations correspond to ON2, ON4, and ON6, respectively, (5, 15, and 25 mm from the bottom of the domain in Figure 3) at the center of the thermistor needle. Lines indicate temperatures at corresponding observation nodes (ON) at the boundary (using numerical solution of Figure 6a).

different conditions, compared with the solution of the infinite line heat source. As expected, temperature responses varied considerably by thermistor location. For all four scenarios, the temperature curves for the thermistors in the sensor body (ON1) or at the tip of the needles (ON7) were very different than for the other thermistors. We conclude that the temperature response in the HPP body (ON1) is very sensitive to epoxy type and whether the body is heated or not. Moreover, body type and heating scenario will affect the temperature responses at the other five locations along the sensor needle, thus affecting analysis of the temperature signals for soil characterization. Similarly, *Ham and Benson* [2004] showed experimentally that temperature measurements are influenced by the difference in thermal properties of the HPP body. Also temperatures at the interface between the HPP sensor body and the soil (ON2) are affected by epoxy type and heating of the epoxy, but are less sensitive than at location ON1. In general, by heating the sensor body, variations in temperature signals along the thermistor needle at ON's 4 and 5 are small and close to the ideal infinite line heat source solution, especially when thermally conductive epoxy is used. Temperature responses at the tip of the thermistor needle (ON7) differ significantly from the other observation nodes because of the heat loss by conduction at the tip of the needle, thus violating the infinite line heat source assumption. Placing thermistors near the end of the sensor needle, when its length is the same as that of the heater needle, will underestimate predicted temperatures leading to erroneous estimates of thermal properties and water fluxes.

[27] In conclusion, as long as the thermistors are located at or near the center of the heater needle, temperatures are suitable for HPP analysis. Similar conclusions were drawn experimentally by *Ham and Benson* [2004] as well as *Mori et al.* [2003, 2005]. This result suggests that sensor needles can be about half the length of the heater element of the HPP to reduce the risk of deflecting needles when inserting them into soils. The thermistors should then be installed at the tip of the sensor needle where measurements deviate least from theoretical values for the infinite line source.

[28] Temperatures presented in Figure 6 were calculated by assuming that the heat transport was unaffected by the presence of sensor needles. Specifically, calculations did not account for the axial heat conduction in the thermistor needle. The impact of the axial conduction for case (a), Figure 6, is shown in Figure 7 where temperatures in the
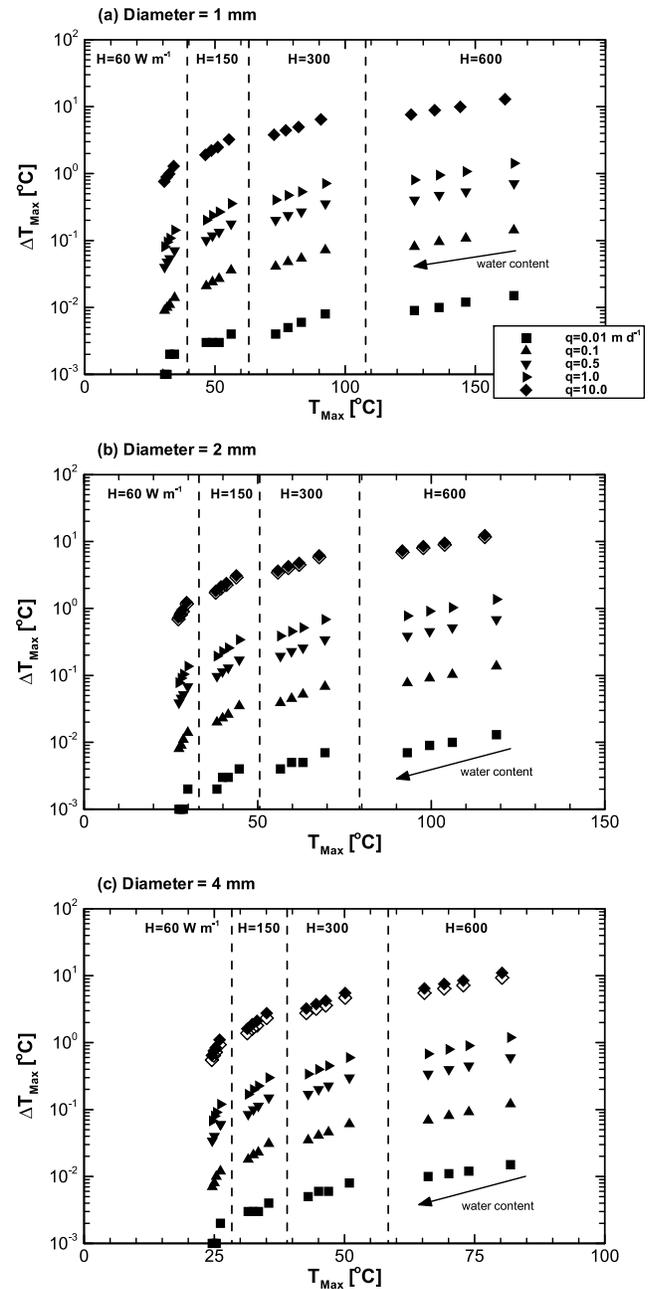

Figure 8. The calculated maximum temperature difference between downstream and upstream thermistors (ΔT_{Max}) as a function of the maximum temperature reached at the heater (T_{Max}) for different heat pulse intensities, water fluxes, and water contents for each probe diameter (Table 2). An arrow indicates increasing water content from 0.3 to 0.6 m^3 m^{-3}. Vertical dashed lines separate data points for different heat pulse intensities. Open symbols for $q = 10.0$ m d^{-1} show results for case where the distance between the heater probe and the sensor probe remained the same (5.5 mm), irrespective of heater diameter.
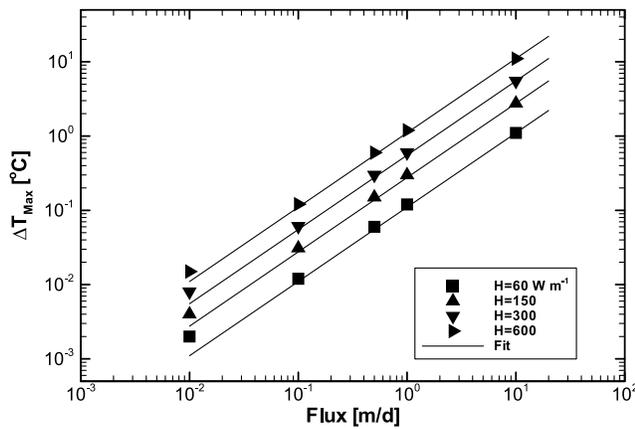
Figure 9. The maximum temperature difference between downstream and upstream thermistors (ΔT_{Max}) as a function of the water flux for four heat pulse intensities (60 to 600 W m^{-1}) with fitted regression lines. Heater needle diameter is 4 mm, and water content is 0.3 m^3 m^{-3}.

center of the thermistor needle are compared to those obtained in Figure 6a. Calculated temperatures in the thermistor needle at three locations corresponding to three ONs (ON2, ON4, and ON6 in Figure 2) are all very close to those imposed at the soil boundary. The overall effect of the axial conduction of heat on temperature changes in the center of the thermistor needle is small enough so that results presented in Figure 6 can be used in further analyses without directly accounting for axial conduction. The radial distance of the center of the needle to its surface is significantly smaller than the axial distances. Since the heat capacity of the soil is significantly larger than that of the sensor, the effect of the axial conduction compared to the radial conduction is relatively small.

4.2. Heater Diameter and Heat Pulse Intensity

[29] Accurate water flux estimations from HPP experiments require accurate temperature differences between downstream (O_d) and upstream (O_u) thermistors (Figure 4) For example, a measurement precision of 0.01°C is needed to estimate a water flux density of 0.06 m d^{-1} [*Ren et al.*, 2000]. Whereas higher heat pulse intensities can be applied to induce larger temperature differences between the O_d and O_u thermistors, the higher temperatures may cause boiling of soil water near the heater. It is therefore that we evaluated the effects of increasing heater diameters and heat pulse intensities, collectively. Figure 8 summarizes the maximum temperature differences between the O_d and O_u thermistors (ΔT_{Max}) as a function of the maximum temperature at the heater boundary (T_{Max}) for different heater diameters, heat pulse intensities, water fluxes, and water content values. Results were obtained with the assumption of perfect thermal contact between the sensor needles and the surrounding soil, realizing that T_{Max} is affected by the contact resistance. Vapor transport was not taken into account, so that temperatures may increase above the boiling point of water [*Ham and Benson*, 2004]. Evaluation of the effects of the coupled water, vapor and energy transport on HPP operation is the subject of section 4.3.

[30] Simulations were conducted for four different water contents (Table 4) for each heat pulse intensity, water flux,

and probe diameter. As the results in Figure 8 show, both the maximum temperature, T_{Max}, and the maximum temperature difference, ΔT_{Max}, decrease as the water content is higher for all possible combinations. This is caused by the larger heat capacity of water, as compared to that of the soil material [*Campbell*, 1985]. Also, as shown by *Ren et al.* [2000] in their analytical solution, for the same heat pulse intensity and water content, the maximum temperature difference (ΔT_{Max}) increases linearly as the water flux is increased (Figure 9). As expected, an increase in the water flux or heat intensity results in larger temperature differences between O_u and O_d thermistors due to heat convection by liquid water.

[31] As the results in Figure 8 indicate, smaller fluxes can be measured at lower water content or higher heat pulse intensity values. Thus the heat pulse intensity needs to be increased to increase the sensitivity of HPP measurements for smaller water fluxes. However, the higher heat pulse intensity may cause vapor flow or temperature-induced liquid water flow, because of the higher soil temperatures generated by the heat pulse. For example, as the results show, applying 600 W m^{-1} heat pulse using the 1-mm-diameter needle can easily boil the soil water around the heater. This means then when larger heat pulses are used in the experimental set up, coupled water, vapor, and energy transport must be considered.
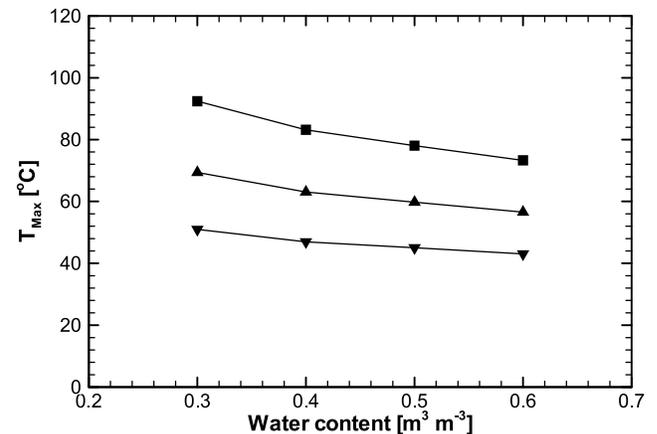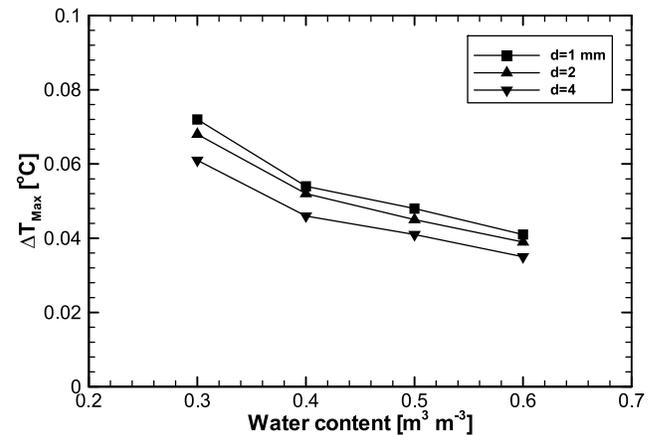

Figure 10. Effects of different diameter heater probes on T_{Max} and ΔT_{Max} for different water content values. Water flux is 0.1 m d^{-1}, and heat pulse intensity is 300 W m^{-1}.
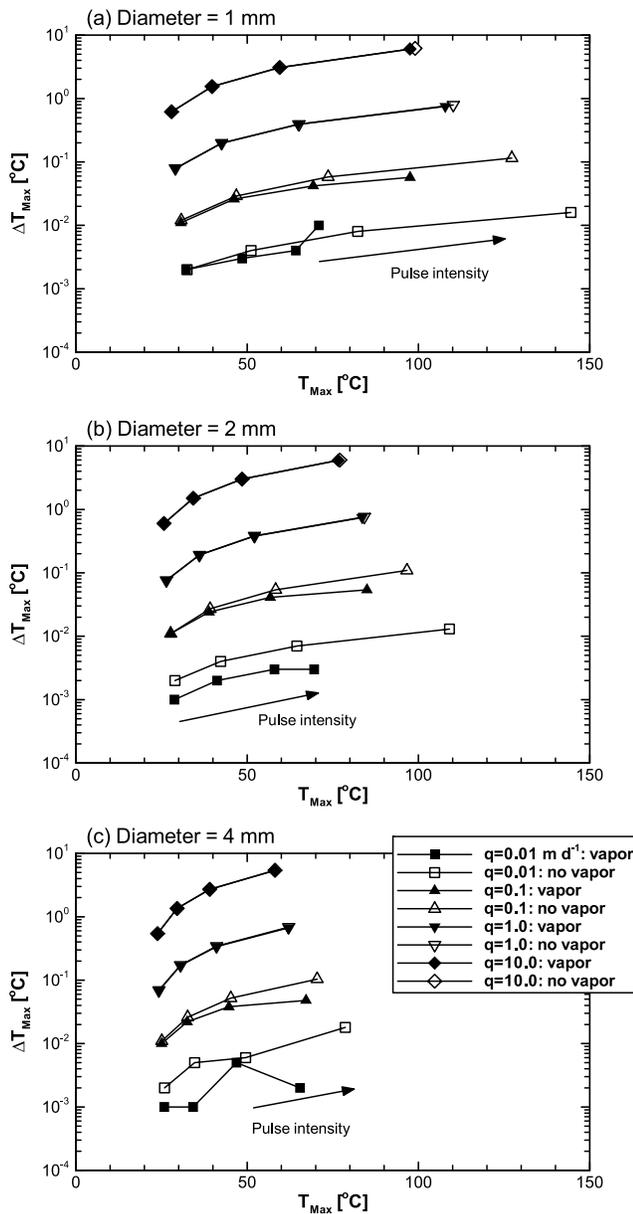
Figure 11. The maximum temperature difference between downstream and upstream thermistors (ΔT_{Max}) as a function of the maximum temperature reached at the heater (T_{Max}), calculated with HYDRUS, with (solid symbols) and without (open symbols) consideration of vapor flow. For each water flux and each heater probe diameter, four different heat pulse intensities of Table 6 are compared. The arrows indicate increasing heat pulse intensity from 60 to 600 W m^{-1}.

[32] The value of T_{Max} can also be reduced by using larger diameter heater needles (Figure 8). Figure 10 shows the impact of changing the heater diameter on ΔT_{Max} and T_{Max} as a function of the water content for a heat pulse intensity of 300 W m^{-1} and a water flux of 0.1 m d^{-1}. While T_{Max} drops significantly, when changing the heater diameter from 1 to 4 mm, ΔT_{Max} remains almost the same (the difference is 0.02°C or less) for a wide range of water content values. This clearly demonstrates the benefit of using a larger diameter heater to reduce $T_{Max,}$ while main-

taining the required ΔT_{Max} resolution. We should mention that larger diameter heater needles can distort water flow [e.g., *Hopmans et al.*, 2002, Figure 6]. This distortion could lead to larger errors when soil hydraulic and thermal properties are estimated using analytically derived solutions. An additional benefit of using the presented numerical approach is that distortion of water flow is taken into account.

[33] The 10 m d^{-1} results of Figure 8 also show the impact of maintaining a constant 5.5-mm distance between the heater and thermistor needle surfaces, irrespective of heater diameter needle (compare open with solid diamond symbols). If this distance is held constant for the three considered heater needle configurations, the heater-thermistor distance between their centers increased from 6.0 mm to 6.5 and 7.5 mm, respectively. While T_{Max} was not affected, ΔT_{Max} slightly dropped for all considered water content and heat pulse intensity values, indicating that an increase of needle distance leads to decreasing sensitivity. In other words, to increase the HPP sensitivity, one may decide to reduce spacing between heater and thermistor needles.

4.3. Vapor Flow

[34] The latent heat of vaporization of water may have a significant effect on predicted temperature responses and estimated soil properties by the HPP method. Mainly because of a lack of available tools, vapor transport was rarely taken into account in HPP studies. Only a few studies [e.g., *Bilskie*, 1994] attempted to use the coupled model of water and energy transport to analyze HPP performance. Recent updates of HYDRUS allow consideration of vapor transport coupled with movement of liquid water and heat in soils [*Saito et al.*, 2006].

[35] The effects of our vapor transport analysis are summarized in Figure 11, where the maximum temperature differences between O_d and O_u thermistors (ΔT_{Max}) are plotted as a function of the maximum temperature at the heater-soil interface (T_{Max}) for different liquid water fluxes, heater diameters and heat flux intensities (Table 6), with and without consideration of temperature-induced vapor transport (compare open with solid symbols). Since the soil system has to be unsaturated for vapor flow to occur, different water contents and water flux values than in section 4.2 were used. Water fluxes and water contents were uniquely linked
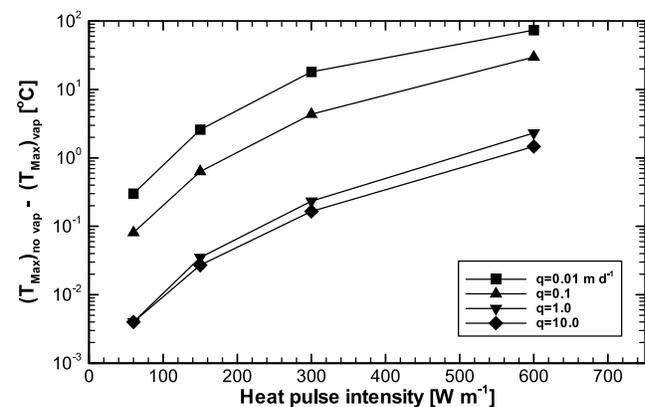

Figure 12. Changes in T_{Max} ($(T_{Max})_{no\ vap} - (T_{Max})_{vap}$), after accounting for vapor flow as a function of the heat pulse intensity for the 1-mm-diameter heater probe predicted with HYDRUS. Subscripts "*vap*" and "*no vap*" indicate consideration of vapor transport.
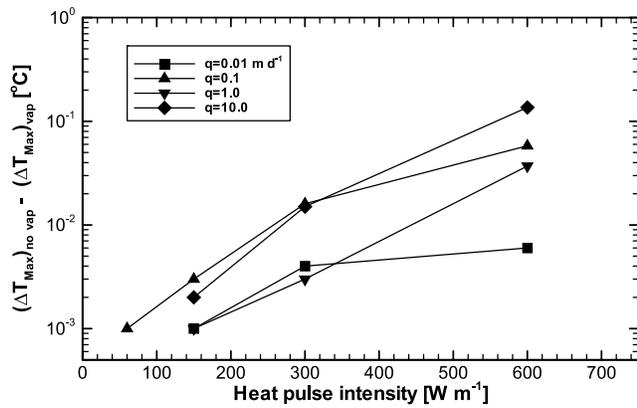
Figure 13. Changes in ΔT_{Max} (($\Delta T_{\mathrm{Max}})_{no\ vap}$ − ($\Delta T_{\mathrm{Max}})_{vap}$) after accounting for vapor flow as a function of the heat pulse intensity for the 1-mm-diameter heater probe predicted with HYDRUS. Subscripts "*vap*" and "*no vap*" indicate consideration of vapor transport.

through the soil hydraulic properties. The impact of considering vapor transport is especially important for a lower water flux (e.g., $q = 0.01$ and 0.1 m d^{-1}) at corresponding lower water contents. Changes in T_{Max} and ΔT_{Max} after accounting for vapor flow as a function of the heat pulse intensity for the 1-mm heater needle are summarized in Figures 12 and 13. Results for fluxes of 0.01, 1.0, and 10.0 m d^{-1} at a heat pulse of 60 W m^{-1} in Figure 13 are not shown as the effect of temperature responses were near 0°C, and below the precision of the numerical calculations. Similar inconsequent results were obtained for heater diameters of 2 and 4 mm (not shown). Figures 12 and 13 demonstrate that while consideration of vapor flow had a significant effect on reducing T_{Max}, the effect on ΔT_{Max} was relatively minor. It is important to realize that ΔT_{Max} was not as much affected by inclusion of vapor transport, as some analytical solutions use temperature differences between upstream and downstream thermistors only [e.g., *Ren et al.*, 2000]. For the smaller heat pulse intensity values, differences between results obtained with the coupled model compared to the standard model were nearly identical for larger water flux values of 1 and 10 m d^{-1} (Figure 11). Not only is vapor diffusion less important for the larger water fluxes, the associated larger water contents decreased the effective vapor diffusivity, because of the corresponding larger tortuosity and lower air content values.

[36] The impact of the needle diameter on changes in T_{Max} and ΔT_{Max}, due to vapor flow for a range of heat pulse intensity values, is shown in Figure 14 for a water flux of 0.1 m d^{-1}. Similar to results presented in Figure 10, while changes in T_{Max} decrease as the heater diameter increases (Figure 14, top), changes in ΔT_{Max} remain the same for different heater diameters (Figure 14, bottom), irrespective of heat pulse intensity. Thus the sensitivity of the HPP to water fluxes is maintained, whether coupled water and energy transport is considered or not, demonstrating the benefits of using larger diameter heating needles.

5. Summary and Conclusions

[37] This study investigated the effects of (1) sensor location and thermal properties of HPP sensor body mate-

rial, (2) the heat pulse intensity and heater diameter, and (3) vapor flow on heat pulse probe (HPP) performance. In addition, the effects of axial heat conductance through thermistor needles were investigated. The following conclusions can be drawn. First, best results are obtained if thermistors are placed away from the sensor body and end of heater needle, preferably midway along the length of the heater needle. If temperatures at locations close to the HPP sensor body are used for the analysis, thermal properties of the HPP sensor body must be carefully taken into consideration. Our results suggest that the length of thermistor needles can be much shorter, as also demonstrated by *Mortensen et al.* [2006], leading to a more rigid heat pulse probe design. Second, using a standard 1-mm heater needle diameter, the temperature difference between the downstream and upstream thermistors increases linearly with an increase in input energy (i.e., heat pulse intensity), potentially leading to a maximum temperature near the heater exceeding 100°C. Soil temperatures can be significantly reduced by using larger diameter heating needles (e.g., 2 or 4 mm), while maintaining the minimum required temperature differences between downstream and upstream sensor needles. Consequently, a higher sensitivity to flux measurements can be achieved when applying larger heat intensities and larger diameter heater needles. Third, consideration of
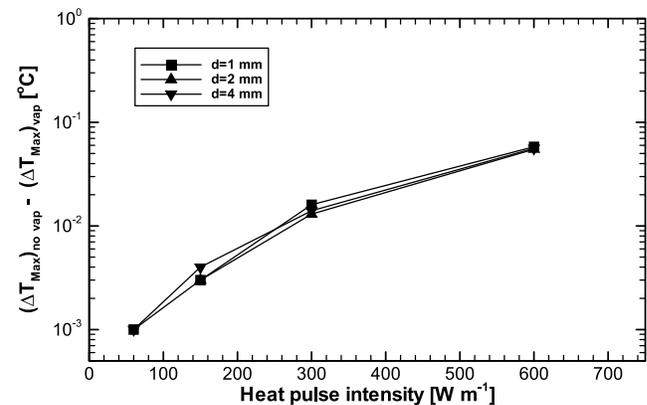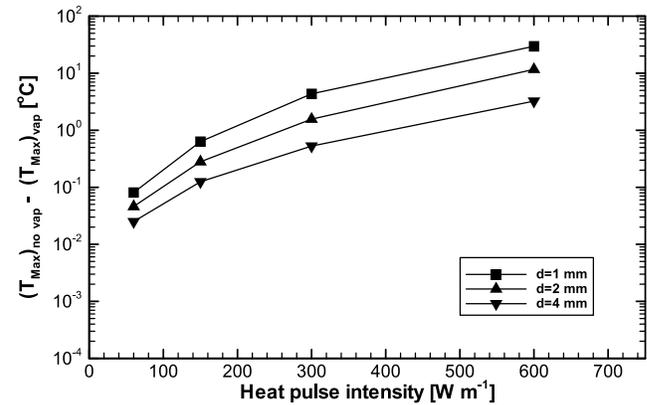

Figure 14. The impact of the heater diameter on changes in T_{Max} and ΔT_{Max}, after accounting for vapor flow as a function of the heat pulse intensity, predicted with HYDRUS. Subscript "*vap*" and "*no vap*" indicate consideration of vapor transport. Water flux density is 0.01 m d^{-1}.

vapor transport showed that the latent heat of vaporization can significantly reduce temperature increases near the heater surface, especially when water flux densities are small. Thus larger heat pulse values can be used, if vapor transport is considered in the HPP analysis. In addition, we also demonstrated that axial heat conductance through the thermistor needles is insignificant for the range of conditions explored in the presented sensitivity analysis.

[38] Another approach to increase HPP sensitivity may be achieved by reducing the distance between heater and thermistor needles or by increasing the heat pulse duration. While decreasing the needle spacing is expected to increase sensitivity, it may increasingly distort water flow, though this can be taken into consideration using numerical solutions. The longer heat pulse duration will increase ΔT_{Max}, while keeping the increase in T_{Max} to an acceptable temperature level. Both numerical and experimental studies will be conducted in the near future to further investigate these additional options for increasing the HPP performance.

References

Bilskie, J. R. (1994), Dual probe methods for determining soil thermal properties: Numerical and laboratory story, Ph.D. dissertation, Iowa State University, Ames.

Bristow, K. L. (1998), Measurement of thermal properties and water content of unsaturated sandy soil using dual-probe heat-pulse probes, *Agric. For. Meteorol.*, 89, 75–84.

Bristow, K. L., G. J. Kluitenberg, and R. Horton (1994), Measurement of soil thermal properties with a dual-probe heat-pulse technique, *Soil Sci. Soc. Am. J.*, 58, 1288–1294.

Campbell, G. S. (1985), *Soil Physics With Basic: Transport Models for Soil-Plant Systems*, Elsevier, New York.

Campbell, G. S., C. Calissendorff, and J. H. Williams (1991), Probe for measuring soil specific heat using a heat-pulse method, *Soil Sci. Soc. Am. J.*, 55, 291–293.

Chung, S.-O., and R. Horton (1987), Soil heat and water flow with a partial surface mulch, *Water Resour. Res.*, 23, 2175–2186.

de Marsily, G. (1986), *Quantitative Hydrogeology: Groundwater Hydrology for Engineers*, Academic, Orlando, Fla.

Gao, J., T. Ren, and Y. Gong (2006), Correcting wall flow effect improves the heat-pulse technique for determining water flux in saturated soils, *Soil Sci. Soc. Am. J.*, 70, 711–717.

Ham, J. M., and E. J. Benson (2004), On the construction and calibration of dual-probe heat capacity sensors, *Soil Sci. Soc. Am. J.*, 68, 1185–1190.

Hopmans, J. W., J. Šimůnek, and K. L. Bristow (2002), Indirect estimation of soil thermal properties and water flux using heat pulse probe measurement: Geometry and dispersion effects, *Water Resour. Res.*, 38(1), 1006, doi:10.1029/2000WR000071.

Kluitenberg, G. J., K. L. Bristow, and B. S. Das (1995), Error analysis of the heat pulse method for measuring soil heat capacity, diffusivity, and conductivity, *Soil Sci. Soc. Am. J.*, 59, 719–726.

Knight, J. H., and G. J. Kluitenberg (2005), Analytical solutions for sensitivity of well tests to variations in storativity and transmissivity, *Adv. Water Resour.*, 28, 1057–1075.

Mori, Y., J. W. Hopmans, A. P. Mortensen, and G. J. Kluitenberg (2003), Multi-functional heat pulse probe for the simultaneous measurement of soil water content, solute concentration, and heat transport parameters, *Vadose Zone J.*, 2, 561–571.

Mori, Y., J. W. Hopmans, A. P. Mortensen, and G. J. Kluitenberg (2005), Estimation of vadose zone water flux from multi-functional heat pulse probe measurements, *Soil Sci. Soc. Am. J.*, 69, 599–606.

Mortensen, A. P., J. W. Hopmans, Y. Mori, and J. Šimůnek (2006), Multi-functional heat pulse probe measurements of coupled vadose zone flow and transport, *Adv. Water Resour.*, 29, 250–267.

Mualem, Y. (1976), A new model for predicting the hydraulic conductivity of unsaturated porous media, *Water Resour. Res.*, 12, 513–521.

Nassar, I. N., and R. Horton (1992), Simultaneous transfer of heat, water, and solute in porous media: I. Theoretical development, *Soil Sci. Soc. Am. J.*, 56, 1350–1356.

Ochsner, T. E., R. Horton, G. J. Kluitenberg, and Q. Wang (2005), Evaluation of the heat pulse ratio method for measuring soil water flux, *Soil Sci. Soc. Am. J.*, 69, 757–765.

Philip, J. R., and D. A. de Vries (1957), Moisture movement in porous materials under temperature gradient, *Eos Trans. AGU*, 38, 222–232.

Ren, T., G. J. Kluitenberg, and R. Horton (2000), Determining soil water flux and pore water velocity by a heat pulse technique, *Soil Sci. Soc. Am. J.*, 64, 552–560.

Saito, H., J. Šimůnek, and B. P. Mohanty (2006), Numerical analysis of coupled water, vapor and heat transport in the vadose zone, *Vadose Zone J.*, 5, 784–800.

Šimůnek, J., and D. L. Suarez (1993), *The UNSATCHEM-2D Code for Simulating Two-Dimensional Variably Saturated Water Flow, Heat Transport, Carbon Dioxide Transport, and Solute Transport With Major Ion Equilibrium and Kinetic Chemistry*, version 1.1, *Res. Rep. 128*, 218 pp., U.S. Salinity Lab., Agric. Res. Serv., USDA, Riverside, Calif.

Šimůnek, J., M. Th. van Genuchten, and M. Šejna (2006), *The HYDRUS Software Package for Simulating Two- and Three-Dimensional Movement of Water, Heat, and Multiple Solutes in Variably-Saturated Media*, version 1.0, technical manual, 241 pp., PC Progress, Prague.

van Genuchten, M. T. (1980), A closed-form equation for predicting the hydraulic conductivity of unsaturated soils, *Soil Sci. Soc. Am. J.*, 44, 892–898.

Wang, Q., T. E. Ochsner, and R. Horton (2002), Mathematical analysis of heat pulse signals for soil water flux determination, *Water Resour. Res.*, 38(6), 1091, doi:10.1029/2001WR001089.

J. W. Hopmans and A. Tuli, Department of Land, Air and Water Resources, University of California, Davis, CA 95616, USA. (jwhopmans@ucdavis.edu; atuli@ucdavis.edu)

H. Saito, Department of Ecoregion Science, Tokyo University of Agriculture and Technology, Fuchu, Tokyo 183-8509, Japan. (hiros@cc.tuat.ac.jp)

J. Šimůnek, Department of Environmental Sciences, University of California, Riverside, CA 92521, USA. (jiri.simunek@ucr.edu)